Pak. J. Bot., 58(12): December 2026.

ARTICLE | DOI: http://dx.doi.org/10.30848/PJB2026-12(21)

IN VITRO AND *IN SILICO* EVALUATION OF ANTIMICROBIAL ACTIVITY OF *FAGONIA ARABICA* AGAINST *ENTEROCOCCUS FAECALIS* ISOLATES FROM ENDODONTIC FAILURE CASES

ANEELA EJAZ[1], MUHAMMAD TAHIR KHAN[2*], HUMA SATTAR[1] AND MUHAMMAD HASSAN[3]

[1]Institute of Molecular Biology and Biotechnology (IMBB), Center for Research in Molecular Medicine (CRiMM), The University of Lahore, 1 KM Defense Road, Lahore 58810, Pakistan, Ph: +92 (0)3344213664
[2]International Center for Interdisciplinary Research in Sciences (ICIRS), The University of Lahore, 1 KM Defense Road, Lahore 58810, Pakistan, Ph: +92 (0)3344213664
[3]University College of Medicine and Dentistry, The University of Lahore, 1 KM Defense Road, Lahore 58810, Pakistan, Ph: +92 (0)3344213664

*Corresponding author's email: muhammad.tahir@cir.uol.edu.pk

Abstract

Enterococcus faecalis (*E. faecalis*) is a multidrug-resistant bacteria causing endodontic failure. The current study aimed to isolate *E. faecalis* from endodontic failure cases and determine its antibiotic susceptibility profile. Moreover, it evaluated the anti- *E. faecalis* potential of *F. arabica.* Fifty samples were collected from patients with endodontic failure. Ten *E. faecalis* isolates were successfully confirmed by 16S rRNA. The disk-diffusion method was used to assess antibiotic susceptibility. Agar well diffusion assay was employed to determine the antibacterial activities of methanolic, ethanolic, and distilled water extracts of *F. arabica*. Sodium hypochlorite (2.5%) and distilled water served as positive and negative controls, respectively. GC–MS analysis was followed by quantum chemical analysis and molecular dynamics (MD) simulation of the selected compounds against the *E. faecalis* Ace protein. Two compounds (C1 and C2) were subjected to quantum chemical analyses, followed by MD simulations. Statistical analysis using linear mixed effects showed significant differences in antimicrobial susceptibility, extract efficacy, and MIC values (p<0.001). All isolates (100%, n = 10) exhibited complete resistance to vancomycin and tetracycline, whereas 80% (n=8) were susceptible to erythromycin. Conversely, 100% of isolates were sensitive to ampicillin and amoxicillin-clavulanate (p<0.001). In agar well diffusion testing, *F. arabica* extracts demonstrated comparable antimicrobial activity ($padj$ = 0.624) to 2.5% sodium hypochlorite ($padj$ <0.01) and distilled water ($padj$ <0.001). The MIC assay demonstrated superior potency (26.42 ± µg/mL) compared to that of methanolic extract and sodium hypochlorite ($padj$ <0.005). GC–MS analysis and MD simulations revealed that C1 is a more favorable inhibitor of Ace protein than C2 (phthalic acid) in *F. arabica*. However, further studies are necessary to assess the clinical efficacy before therapeutic applications.

Key words: *E. faecalis; Fagonia arabica;* MIC; Endodontic failure

Abbreviations: *E. faecalis* = *Enterococcus faecalis*; *F. arabica* = *Fagonia arabica*; PCR = Polymerase chain reaction; GC-MS analysis = Gas Chromatography-Mass Spectrometry; MIC = Minimum Inhibitory Concentration; ZOI = Zone of Inhibition; kcal/mol = kilocalories per mole; EDTA = Ethylenediaminetetraacetic acid; UOL = The University of Lahore; IRB = Institutional Review Board; PCR = Polymerase chain reaction; SPSS = Statistical Package for the Social Sciences.

Introduction

Endodontic treatment failure remains a substantial clinical challenge, despite advancements in disinfection practices and instrumentation techniques. The reported prevalence of endodontic failure ranges from 27% to 78.8%, primarily due to the persistence of intracanal microorganisms that are difficult to eradicate (Iqbal, 2016). There are several microorganisms responsible for secondary and persistent endodontic disease; however, *Enterococcus faecalis (E. faecalis*) has consistently been identified as the predominant pathogen responsible for endodontic failure (Alghamdi & Shakir, 2020; Aydın *et al.,* 2025).

Enterococcus faecalis is an anaerobic Gram-positive bacterium. Its persistence within the root canal is due to various virulence factors. It can penetrate deeply into the dentinal tubules, adhere to collagen-rich dentin surfaces, and establish highly resistant biofilms that are difficult to remove (Kohi *et al.,* 2026). The collagen-binding proteins, particularly Ace (adhesion of collagen from *Enterococci*), are responsible for the dentinal adhesion of *E. faecalis* (Hubble *et al.,* 2003). Furthermore, its ability to survive under harsh intracanal conditions, including nutrient deprivation, low oxygen tension, and alkaline environments, enables long-term persistence and increases the probability of treatment failure (Nallamilli *et al.,* 2026).

Conventional endodontic disinfection techniques are typically based on intracanal instrumentation, irrigation, and intracanal medication. The intracanal irrigants include sodium hypochlorite, ethylenediaminetetraacetic acid (EDTA), and chlorhexidine. Different percentages of sodium hypochlorite are used in endodontics; however, 2.5% is considered a gold standard (Kini *et al.,* 2015). Although these agents have broad-spectrum antimicrobial activity, their limited ability to eliminate biofilm-forming *E. faecalis* leads to persistent infection and treatment failure. Thus,

Received: 09-05-2026 | Revised: 28-07-2026 | Accepted: 04-08-2026 | Online: 20-08-2026

significant concerns regarding antimicrobial resistance have resulted in the formulation of novel phytochemical-based remedies (Zou *et al.,* 2024; Zubair *et al.,* 2025).

Medicinal plants and their phytochemicals have long been used in dentistry for their antimicrobial, anti-inflammatory, biocompatibility, and cost-effectiveness (Budala *et al.,* 2023). As compared to conventional antimicrobial agents, herbal products offer advantages such as fewer adverse effects, reduced risk of resistance development, and improved accessibility. Many herbal plants, such as Neem, Triphala, and Propolis, have been investigated as intracanal medicaments and root canal irrigants, with promising antimicrobial activity (Mohsin *et al.,* 2025).

Among medicinal plants with potential therapeutic value, *Fagonia arabica* (*F. arabica*), commonly known as Dhamassa, has attracted increasing scientific interest. This flowering plant species belongs to the Zygophyllaceae family. It has been employed in Ayurvedic medicine to treat different inflammatory and infectious diseases (Abobaker, 2015). Previous studies have demonstrated that *F. arabica* has antithrombotic, anticancer, antioxidant, and antibacterial activities due to its various phytochemical constituents, including flavonoids, alkaloids, terpenoids, and phenolic compounds (Iftikhar *et al.,* 2022; Mahmoud *et al.,* 2025).

However, despite its documented antimicrobial potential, evidence regarding its effectiveness against *E. faecalis* associated with persistent endodontic infection remains limited. Moreover, the mechanisms of their interactions with bacterial virulence factors involved in endodontic persistence have not been adequately explored. Hence, this study was designed to isolate and molecularly confirm *E. faecalis* isolated from patients with endodontic treatment failure. The antibacterial activities of ethanol, methanol, and distilled water extracts of *F. arabica* were evaluated against the bacterial isolates.

In addition, the phytochemical composition of its active constituents was determined through GC-MS analysis. The compounds identified by the GC-MS were used as ligands for molecular docking and molecular dynamics (MD) simulations to predict their binding affinities and potential interactions with the Ace protein of *E. faecalis*, thereby providing insights into their possible antimicrobial activity (Srimyvizhy *et al.,* 2026).

Materials and Methods

The study was conducted at the dental hospital of the University of Lahore (UOL) from April 2023 to December 2024. It was ethically approved by the IMBB Review Board of the University of Lahore (IMBB/BBBC/23/140).

Study design and sample collection: In this study, fifty patients diagnosed with endodontic failure, both clinically and radiographically by an endodontist, were selected through purposive sampling. The clinical findings included pain, swelling, and discomfort while chewing in a previously endodontically treated tooth. The exclusion criteria were canal calcifications, perforations, and missed canals. Written informed consent was obtained from each patient.

The sample size was determined using 80% statistical power and an anticipated endodontic failure rate of 14.5%. The level of significance was $\alpha = 5$. All patients aged ≥ 18 years were included.

A rubber dam was used to isolate the teeth. The crown was disinfected with 2.5% sodium hypochlorite for 5 seconds. An access cavity was created using a bur. The Gutta-percha (GP) points were removed with a sterile R25 file (VDW, Munich, Germany). A radiograph was obtained to determine the working length. The sample was taken with the help of two paper points (Dentsply Maillefer, Ballaigues, Switzerland) and inserted into Eppendorf tubes containing 1.0 mL of VMGA III transport medium. Samples were inoculated onto Slanetz and Bartley (Sigma-Aldrich, Cat. No. 105262, St. Louis, USA) *E. faecalis* selective agar media (Hoque *et al.,* 2023).

Culture and primary identification: The tubes were vortexed for 1 minute on an anaerobic workstation and streaked onto agar plates. The initial characterization of *E. faecalis* was based on colony morphology. The size, shape, and color of the surface textures were observed (Fig. 1). The isolates were purified by subculturing and confirmed by Gram staining and catalase testing (negative for *E. faecalis*) (Francisco *et al.,* 2021).

Molecular identification: DNA was extracted and purified from *E. faecalis* isolates using the GeneAll® Exgene™ kit. The manufacturer's instructions were followed. DNA concentration (absorbance at 260 nm) concentration was measured using a spectrophotometer (Thermo Fisher Scientific; NanoDrop 2000; Wilmington, DE, USA) was used for measuring the. The 16S rRNA gene was amplified using specific primers described by (Skotniczny & Satora, 2023).

F: 5′-AGAGTTTGATCCTGGCTCAG-3′
R: 5′- AAGGAGGTGATCCAGCCGCA -3′

Polymerase Chain Reaction (PCR) amplification was achieved using a GenePro (Bioer Technology, Hangzhou, China). The PCR was conducted as follows:

The denaturation was performed initially at 94°C for 10 minutes. Then, 35 cycles of denaturation were completed at 94°C for 1 minute, followed by annealing at 56°C for 1 minute and then extension at 72°C for 2 minutes. The final extension was achieved at 72°C for 10 minutes. The amplified DNA segments were examined using a standard laboratory technique: 1.5% agarose gel electrophoresis was performed. PCR-positive isolates were sequenced by Sanger sequencing, and FASTA sequences were evaluated with the NCBI BLAST tool for identification. Accession numbers were obtained for all identified isolates (Francisco *et al.,* 2021).

Preparation of plant extracts: *Fagonia arabica* plants were collected from the Cholestan Desert in Southern Punjab, Pakistan. The plant specimens were sent to the Government College University, Lahore, for taxonomical identification (GC. Herb. Bot. 3940). The whole plant was shade-dried. A mechanical grinder was used to convert it into powder form. The powder (100 g) was dissolved in 500 mL of methanol and ethanol for seven days. The samples were filtered through Whatman paper #1, evaporated using a rotary evaporator, lyophilized, and kept at 4°C for further use (Tsimidou, 2023). A distilled water extract was prepared following the same procedure.

Antimicrobial susceptibility assay: The antimicrobial susceptibility assay determined the resistance patterns of the isolated *E. faecalis* strains, which provides epidemiological information on the isolates and allows the assessment of whether *F. arabica* exhibits antimicrobial activity against clinically relevant, potentially resistant isolates.

The culture sensitivity testing was performed using the Kirby-Bauer disk diffusion method following the Clinical and Laboratory Standards Institute (Anon., 2024) guidelines. Bacterial suspensions were standardized to a 0.5 McFarland turbidity standard and spread uniformly on the agar surface. The antibiotic disks of ampicillin (10 µg), erythromycin (15 µg), amoxicillin-clavulanate (30 µg), vancomycin (30 µg), and tetracycline (30 µg) were incubated at 37°C for 24 hours. The clear zones of inhibition were measured, and isolates were classified as sensitive, intermediate, or resistant based on the CLSI (2024) interpretive standards (Azad *et al.,* 2020). The zones were categorized according to the CLSI-2024 manual (Kalin *et al.,* 2023).

Antimicrobial activity of plant extracts: The antimicrobial activity of *F. arabica* extracts was performed using agar well diffusion assay. A bacterial suspension equivalent to the 0.5 McFarland standard (approximately 1.5×10^8 CFU/mL) was equally spread onto Mueller–Hinton agar plates with a sterile cotton swab. Subsequently, 6 mm diameter wells were prepared with sterilised cork borers. The dried crude methanolic, ethanolic, and aqueous plant extracts were reconstituted with the respective solvent to get the final concentration of 100 mg/mL for each extract. A volume of 100 µL of each extract (10 mg per well) was dispensed into the respective wells. Sodium hypochlorite (2.5%) and distilled water were employed as the positive control and the negative control. The well plates were incubated at 37°C for 24 hours. Thereafter, the zone of inhibition (ZOI) of every well was measured. The experiments were recorded in triplicate, and the mean values were documented (Ali *et al.,* 2022).

The minimum inhibitory concentration (MIC): A broth dilution test was used to evaluate the MIC using a broth microdilution assay in a 96-well microtiter plate according to CLSI guidelines (CLSI 2024). Two-fold serial dilutions of each plant extract (100 µL) were made across the plate in Mueller-Hinton Broth (MHB) in 96-well microtiter plates containing 100 µL of nutrient broth. Approximately 1.5×10^8 CFU/mL (0.5 McFarland) bacterial suspensions were added to each well. To attain a final concentration of approximately 5×10^5 CFU/mL in each well, it was further diluted in MHB. Optical density (OD) was determined at 630 nm at 0 and 24 hours. The lowest inhibitory concentration (MIC) was determined with no visible growth (Muhammad *et al.,* 2025).

GC-MS analysis: Gas chromatography–mass spectrometry (GC–MS) was used to identify the bioactive components of *F. arabica*. A Clarus 500 PerkinElmer (AutoSystem XL) Gas Chromatograph was coupled with a TurboMass Gold PerkinElmer TurboMass 5.1 mass spectrometer. Separation was performed by using an Elite-1 capillary column (100% dimethylpolysiloxane; 30 m × 0.25 mm internal diameter × 1 µm film thickness). The temperature of the oven was originally retained at 70°C for 3 minutes, followed by an increase in temperature at 10°C/min to 300°C and held for 9 minutes. Helium gas was used as the carrier at a flow rate of 1.5 mL/min. A 1 µL aliquot of the sample was injected in split mode (10:1), and the temperature was kept at 250°C. The mass spectrometer operated in electron ionization (EI) mode at 70 eV. The interface temperatures and ion source were kept at 230°C and 240°C, respectively. Mass spectra were acquired over the range of 40–700 m/z. The total runtime was 35 minutes, with an MS start time and a solvent delay of 3 minutes. Phytochemical components were identified by the comparison of the mass spectra with the National Institute of Standards and Technology (NIST) Mass Spectral Library (Version 11). The identification was based on retention characteristics and spectral matching (Ghosh *et al.,* 2015).

Density functional theory (DFT) analysis of compounds: The structures of Phthalic acid (C1) and Pyrazine-2,6-diamine (C2) were drawn using GaussView 6.0.16. DFT was performed for geometry optimization. The APFD functional and 6-311+G (2d, p) basis set were implemented in Gaussian. The molecular electrostatic potential (MEP) maps were computed, and frontier molecular orbital (FMO) calculations, including highest occupied molecular orbitals and lowest unoccupied molecular orbitals (HOMO and LUMO) energies was performed with optimized geometry.

Molecular docking: It was executed to assess the binding interactions between the identified phytochemicals and the bacterial target, the collagen-binding MSCRAMM adhesin Ace protein of *E. faecalis*. The crystal structure of the protein was retrieved from the Protein Data Bank (PDB ID: 2Z1P). The structures of ligands were downloaded from the PubChem database in SDF format. Before docking, both protein and ligand structures were prepared using the preparation wizards in UCSF Chimera. Excess water molecules were eliminated from the protein structure. Hydrogen atoms were added to both the ligands and protein to simulate physiological pH conditions. Bond orders were corrected, and missing side chains or loop regions were added.

Ligand structures and proteins were docked using the AutoDock Vina plugin integrated within UCSF Chimera (Butt *et al.,* 2020). The docking grid was centered on the putative collagen-binding trench located at the interface of the N1 and N2 subdomains of the Ace protein, encompassing functionally important residues. The grid box was selected as follows: Center; X: 53.833, Y: 78.2057, Z: 133.9899 Å, and grid spacing of 1.0 Å. The protein-ligand residue interactions were analyzed using Ligplot$^+$ (v.2.2.8) (https://www.ebi.ac.uk/thornton-srv/software/LigPlus/) (Wallace *et al*., 1995).

Molecular dynamics simulation (MD) simulation: The docked complexes of the Ace protein (PDB ID: 2Z1P) with the selected lead ligand compound were simulated using GROMACS 2021.4, an MDS software, for a time duration of 200ns. The 1GTV was also simulated in the native system without a ligand (apo-1GTV) for 200 ns to evaluate and compare the conformational changes, stability, interaction mechanisms, and other thermodynamic properties with the docking complexes of 1GTV-ligands. Topology files for all lead compounds (ligands) were generated using SwissParam (https://old.swissparam.ch/). The protein topology files (protein alone and along with ligands) were prepared using the CHARM27 all-atom

force field and TIP3P water model. The native protein and complexes were then centered in cubic and triclinic boxes of volumes 390.61 nm^3 and 236.76 nm^3, with 1.0 nm box edges, and 11990 and 7107 simple point charge (SPC) 216 water molecules, respectively. The steepest descent algorithm was used for vacuum minimization (50000 steps), followed by solvent energy minimization. The addition of two Na ions neutralized the native protein system. For the energy minimization step, the steepest descent method was used at constant volume, with 1 atm pressure and 300 K temperature, over 50000 steps. In the next step, the system was equilibrated under NVT (number of atoms, constant volume, and temperature) and NPT (number of atoms, constant pressure, and temperature) conditions sequentially for 1000 ps (1 ns) each for all systems. The final step was the performance of MD simulations for 100 ns for both systems, and the resulting trajectories were used for analysis.

Quantum chemical analysis of C1 and C2: The most fundamental variables in quantum chemical research are the energies of the HOMO-LUMO (π donor and π acceptor). The chemical behavior of a compound was determined by reactivity and stability (energy gaps and orbitals). The HOMO-LUMO energy gap serves as the basis for the interaction capability or reactivity and can disclose the inhibitory effects of compounds. The high HOMO-LUMO gap renders the compounds less reactive, hard, and stable. The LUMO acts as a nucleophilic and the HOMO as an electrophilic attracting group during binding and reactivity. The chemical reactivity and kinetic stability are measures of the energy gap.

Statistical analysis

Individual bacterial isolates served as an individual experimental unit. A total of 10 bacterial isolates ($n = 10$) were evaluated across all antimicrobial treatments. Each assay was performed in triplicate to ensure reproducibility. Data were reported as Mean ± Standard deviation (SD). The Shapiro-Wilk test was employed to determine the normality of the distribution. Homogeneity was measured using Levene's test. Non-independence within the same 10 isolates was addressed by analyzing the data using a Linear Mixed-Effects Model (LMM). Whereas the treatment was labeled as a fixed factor and isolate was assigned as a random blocking factor. Pairwise post-hoc comparisons between treatment groups were achieved using Tukey's Honest Significant Difference (HSD) test with adjusted p-values ($p_{\text{adj}} < 0.05$). All statistical analyses were completed using IBM SPSS Statistics for Windows, Version 26.0 (IBM Corp., Armonk, N.Y., USA).

Results

Biochemical identifications: To increase the likelihood of obtaining clinically significant isolates from cases of endodontic failure. A total of 50 patients were selected. Bacterial growth was observed in 20 primary culture plates, and ten were identified as *E. faecalis.* Ten representative *E. faecalis* isolates were selected for a detailed examination. These isolates were selected based on specific criteria, including purity, successful molecular confirmation, and consistent growth patterns. All isolates were confirmed as *E. faecalis* based on their appearance on Slanetz and Bartley agar (Fig. 1), and the catalase test was negative.

Molecular confirmation of *E. faecalis* isolates: All isolates were amplified using 16S rRNA primers. Gel electrophoresis revealed a clear band of approximately 1500 bp, confirming the presence of *E. faecalis* (Fig. 1). Nanodrop® (Thermo Fisher Scientific, London, UK) was used to evaluate the DNA quality from fresh broth cultures of isolates. Sanger sequencing and BLAST analyses were performed to confirm *the presence of E. faecalis.* All 16S rRNA sequences of *E. faecalis* were submitted to GenBank, and accession numbers were acquired as PP886468-PP886477 (Hassoun & Mohammed, 2022).

Antimicrobial sensitivity assay and Zone of inhibition: Antibiotic susceptibility tests and ZOI diameters of 10 isolates were evaluated against five selected antibiotics according to the CLSI-2024 manual (Table 1). There was a significant difference in the overall antibacterial activity of all antibiotics (p_{adj} <0.05). The results of the present study showed that all isolates (100%) were completely susceptible to ampicillin and amoxicillin-clavulanate (ZOI ≥ 17). The ZOI of ampicillin ranged from (17.00 ± 0.06) to (19.10 ± 0.70) mm, while the ZOI of amoxicillin-clavulanate ranged from a minimum of 17.05 ± 0.41 to 20.08 ± 0.15 mm, and all isolates were susceptible to amoxicillin-clavulanate. 10/10 (100% of isolates) were resistant to vancomycin and tetracycline (ZOI ≤ 14 m, whereas vancomycin demonstrated ZOI ranging from (0.00±0.00) to (11.07 ± 0.45) mm, and tetracycline to (14.06 ± 0.35). respectively. Erythromycin demonstrated variable resistance, with 8/10 (80%) of isolates resistant (ZOI ≤ 13 mm) and two isolates 2/10 (20%) showed intermediate susceptibility (ZOI 12-14 mm), ranging from 10.03 ± 0.15 to 14.06 ± 0.35 (Table 1, Fig. 1). Pairwise post-hoc comparison with Tukey's HSD confirmed that the mean ZOI of ampicillin and amoxicillin clavulanate (p *adj*<0.05) was significantly greater as compared to other antibiotics.

Agar well diffusion assay of *F. arabica* extracts: The antimicrobial activity of methanolic, ethanolic, and distilled water extracts, 2.5% sodium hypochlorite positive control, and distilled water negative control against *E. faecalis* isolates is summarized in Table 2. The linear model mixed effect model analysis demonstrated a significant difference (p<0.001) among all extracts. However, the ethanolic plant extract demonstrated the highest mean ZOI (12.98 ± 2.51 mm), which ranged from (9.00 ± 1.00) to (16.5 ± 1.00). The methanolic extract demonstrated comparable (12.11 ± 1.83 mm), ranging from (9.0 ± 1.07) to (15.0 ± 2.09).

Pairwise post-hoc comparisons by Tukey's HSD test showed not statistically significant (*padj*= 0.624) difference between the mean ZOIs of the ethanolic and methanolic extracts. However, both extracts exhibited significantly larger inhibition zones than 2.5% sodium hypochlorite (9.26 ±3.39 mm; *p-adj* <0.01) and negative control (0.80 ± 1.41 mm*; p-adj* < 0.001). The distilled water extract showed negligible mean activity (0.856 ± 1.41 mm). It demonstrated less activity in only three isolates (PP886471, PP886473, and PP886474) (Table 2).

Minimum inhibitory concentration (MIC): The MIC values of ethanolic, methanolic, and 2.5% sodium hypochlorite extracts in clinical *E. faecalis* isolates (PP 886468 to PP886477) are presented in Table 3.

A Linear Mixed-Effects Model demonstrated treatment as a fixed factor and isolate as a random blocking factor to account for non-independence. There was a statistically significant ($p<0.001$) effect of methanol, ethanol, and 2.5% sodium hypochlorite according to the linear mixed-effects model. The ethanol extract exhibited a significantly lower MIC (overall mean: 26.42 ±10.74 µg/mL) than the methanolic extract (49.95±13.56 µg/mL; $p_{adj} = 0.002$) and 2.5 % sodium hypochlorite (53.18 ± 18.12 µg/mL; p_{adj} <0.00). There was no statistically significant difference between the MIC values of the methanolic extract and 2.5% sodium hypochlorite. ($p_{adj} = 0.781$). The ethanolic extract consistently exhibited a lower inhibitory concentration, particularly against isolates PP886472, PP886473, and PP886477 (15.52 ± 0.00 to 15.61 ± 0.00 µg/mL.

Data are presented as mean ± standard deviation across the replicates (n = 3) for each of the 10 biological isolates. Analyzed using a Linear Mixed-Effects Model (LMM) with treatment as a fixed factor and isolate as a random blocking factor. Overall treatment means sharing a common superscript letter (a, b, c, d, e) are not significantly different ($p>0.05$), whereas means with different superscripts differ significantly ($p>0.05$), based on Tukey's HSD post-hoc test for multiple comparisons.

Gas chromatography-mass spectrometry (GCMS) analysis: The analysis results revealed that the major organic components in the ethanolic extract were formic acid (90.76%), methyl diselenide (4.65%), methyl (Z)-octadec-9-enoate (1.98%), di-n-octyl phthalate (1.09%), Pterin-6-carboxylic acid (0.63%), and carbamic acid, N-cyanomethyl propanamide-2yN-cyanomethyl propanamide-2y (0.49%).

In the methanolic extract of *F. arabica,* the major organic molecules identified by GC-MS analysis were 6-fluoro-2-[4-[(E)-2-phenylethenyl] phenyl] quinoline-4-carbox (27.99%), propenamide (19.9%), phthalic acid, di (hept-3-yl) ester (5.48%), 2,2-dichloroacetamide (1.47%), and pyrazine-2,6-diamine (1.38%).

In the ethanolic extract, formic acid was the most abundant compound (90.76%), followed by methyl diselenide (4.65%), and cyanomethylpropanamide-2y was the least abundant (0.49%). In the methanolic extract, the compound present at the highest concentration was 6-fluoro-2-[4-[(E)-2-phenylethenyl] phenyl] quinoline-4-carbon, followed by propanamide (19.9%), with pyrazine-2,6-diamine at the lowest concentration (1.38%). The results of the GC-MS analysis of the ethanolic and methanolic extracts of *F. arabica* are presented in Table 4. The chromatograms of these extracts are presented in the Supplementary File S1.

Table 1. *In vitro* antibiotic susceptibility testing and zone of inhibition measurements for the bacterial strains.

S. No.	Antibiotics disc concentration	Zone of inhibition (ZOI (mm))									
		PP886468.1	**PP886469.1**	**PP886470.1**	**PP886471.1**	**PP886472.1**	**PP886473.1**	**PP886474.1**	**PP886475.1**	**PP886476.1**	**PP886477.1**
1.	Tetracycline (30 µg)	13.02 ± 0.02^{bc}	16.08 ± 0.57^{e}	14.08 ± 0.25^{cd}	12.03 ± 0.17^{ab}	13.08 ± 0.15^{bc}	14.09 ± 0.07^{cd}	11.10 ± 0.09^{a}	13.38 ± 0.15^{bc}	11.06 ± 0.10^{a}	12.32 ± 0.06^{ab}
2.	Amoxicillin clavulanate (30 µg)	20.05 ± 0.14^{c}	18.06 ± 0.43^{ab}	19.08 ± 0.26^{bc}	17.05 ± 0.41^{a}	18.06 ± 0.06^{ab}	20.08 ± 0.15^{c}	18.05 ± 0.11^{ab}	17.07 ± 0.10^{a}	19.06 ± 0.25^{bc}	18.04 ± 0.05^{ab}
3.	Vancomycin (30 µg)	7.03 ± 0.00^{b}	0.00 ± 0.00^{a}	0.00 ± 0.00^{a}	0.00 ± 0.00^{a}	0.00 ± 0.00^{a}	0.00 ± 0.00^{a}	0.00 ± 0.00^{a}	0.00 ± 0.00^{a}	0.00 ± 0.00^{a}	0.00 ± 0.00^{a}
4.	Erythromycin (15 µg)	13.05 ± 0.03^{cd}	14.06 ± 0.35^{d}	13.09 ± 0.25^{cd}	10.03 ± 0.15^{a}	12.02 ± 0.32^{bc}	13.04 ± 0.11^{cd}	11.07 ± 0.45^{ab}	12.08 ± 0.07^{bc}	14.04 ± 0.06^{d}	13.03 ± 0.1^{cd}
5.	Ampicillin (10 µg)	17.72 ± 0.45	18.02 ± 0.53^{bc}	17.00 ± 0.06^{a}	19.00 ± 0.52^{cd}	17.83 ± 0.20^{b}	18.66 ± 0.55^{bc}	18.00 ± 0.29^{bc}	$17.41 \pm 0.5\ 2^{ab}$	19.10 ± 0.70^{d}	17.80 ± 0.26

Table 2. Mean and standard deviation of antimicrobial activity of *F. arabica L* plant extracts by Agar Well Diffusion test.

S. No.	Antimicrobial activity	Zone of inhibition (ZOI (mm)										
		PP886468	PP886469	PP886470	PP886471	PP886472	PP886473	PP886474	PP886475	PP886476	PP886477	Overall mean
1.	Methanolic extract	13.6 ± 1.55	12.6 ± 1.55	11.0 ± 1.05	9.0 ± 1.07	14.0 ± 1.09	10.0 ± 1.10	11.0 ± 1.12	12.3 ± 2.08	15.0 ± 2.09	12.6 ± 1.52	12.11 ± 1.83^{a} mm
2.	Ethanolic Plant extract	14.3 ± 2.08	16.0 ± 2.60	10.0 ± 1.00	16.5 ± 1.00	14.0 ± 1.00	11.0 ± 1.527	13.0 ± 1.527	11.0 ± 1.527	15.0 ± 1.00	9.0 ± 1.00	12.98 ± 2.51^{a}mm
3.	Distilled water extract	0.0 ± 0.00	0.0 ± 0.00	0.0 ± 0.00	4.0 ± 1.00	0.0 ± 0.00	2.0 ± 1.50	2.6 ± 1.00	0.0 ± 0.00	0.0 ± 0.00	0.0 ± 0.00	0.86 ± 1.41^{c} mm
4.	2.5% Sodium hypochlorite	6.0 ± 1.00	12.0 ± 1.00	15.0 ± 1.00	14.0 ± 1.00	10.0 ± 1.00	5.8 ± 1.00	7.6 ± 1.50	5.6 ± 1.50	9.6 ± 1.50	7.0 ± 1.00	9.26 ± 3.39^{b} mm
5.	Distilled water (-ve control)	0.0 ± 0.00	0.0 ± 0.00	0.0 ± 0.00	0.0 ± 0.00	0.0 ± 0.00	0.0 ± 0.00	0.0 ± 0.00	0.0 ± 0.00	0.0 ± 0.00	0.0 ± 0.00	0.00 ± 0.00^{c} mm

Note: Data represent the Mean ± Standard Deviation across replicates (n= 3) for each of the 10 isolates (n = 10). A Linear Mixed-Effects Model (LMM) was employed, with treatment as a fixed factor and isolate as a random blocking factor. The common superscript letters (a, b, c, d) are not significantly different ($p_{adj} \geq 0.05$). Means with different superscripts differ significantly ($p_{adj} \leq 0.05$) based on Tukey's HSD post-hoc test for multiple comparisons

Table 3. Minimum inhibitory concentration (MIC; mean ± standard deviation) of ethanolic and methanolic extracts and 2.5% sodium hypochlorite against *E. faecalis* isolates.

Isolates	Ethanolic extract	Methanolic extract	2.5% Sodium hypochlorite
PP886468	31.15 ± 0.00	62.4 ± 0.00	64.5 ± 0.00
PP886469	20.82 ± 9.02	41.66 ± 18.04	30.25 ± 0.00
PP886470	30.25 ± 0.00	62.4 ± 0.00	83.32 ± 36.08
PP886471	41.65 ± 18.04	41.66 ± 18.04	62.4 ± 0.00b
PP886472	15.52 ± 0.00	62.4 ± 0.00	31.24 ± 0.00
PP886473	15.52 ± 0.00	62.4 ± 0.00	41.66 ± 18.04
PP886474	20.82 ± 9.02	31.24 ± 0.00^{a}	62.4 ± 0.00b
PP886475	31.24 ± 0.00	62.4 ± 0.00	31.24 ± 0.00
PP886476	41.65 ± 18.04	41.66 ± 18.04	62.4 ± 0.00
PP886477	15.61 ± 0.00	31.24 ± 0.00	62.4 ± 0.00
Overall mean	26.65 ± 10^{a}	49.95 ± 13.56^{b}	53.18 ± 18.12^{b}

Note: Data are presented as mean ± standard deviation of $n = 3$ technical replicates across 10 biological isolates ($n = 10$). Analyzed using a Linear Mixed-Effects Model (LMM) with Treatment as a fixed factor and Isolate as a random blocking factor (Value, $p < 0.001$). Overall treatment means with different superscript letters (a, b) differ significantly ($p_{adj} < 0.05$) based on Tukey's HSD post-hoc

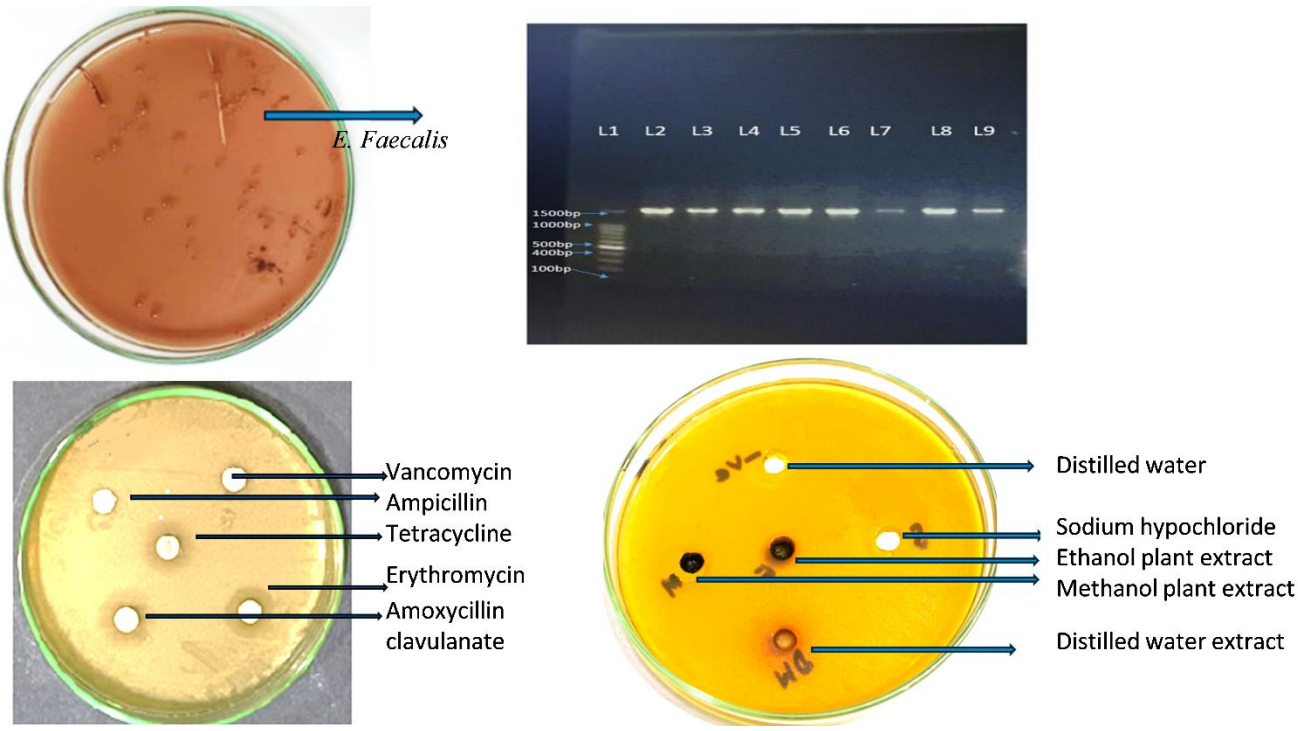

Fig. 1. Culture characteristics of *E. Faecalis.* **Top right:** PCR Confirmation of *E. faecalis* isolates. L1: Ladder; L2 to L9: Samples. Bottom left: Inhibition zones of vancomycin, ampicillin, tetracycline, erythromycin, and amoxicillin-clavulanate. Bottom right: Zone of inhibition of methanol, ethanol, and distilled water (DW) plant extracts, sodium hypochlorite positive control (+ve), and distilled water negative control (-ve).

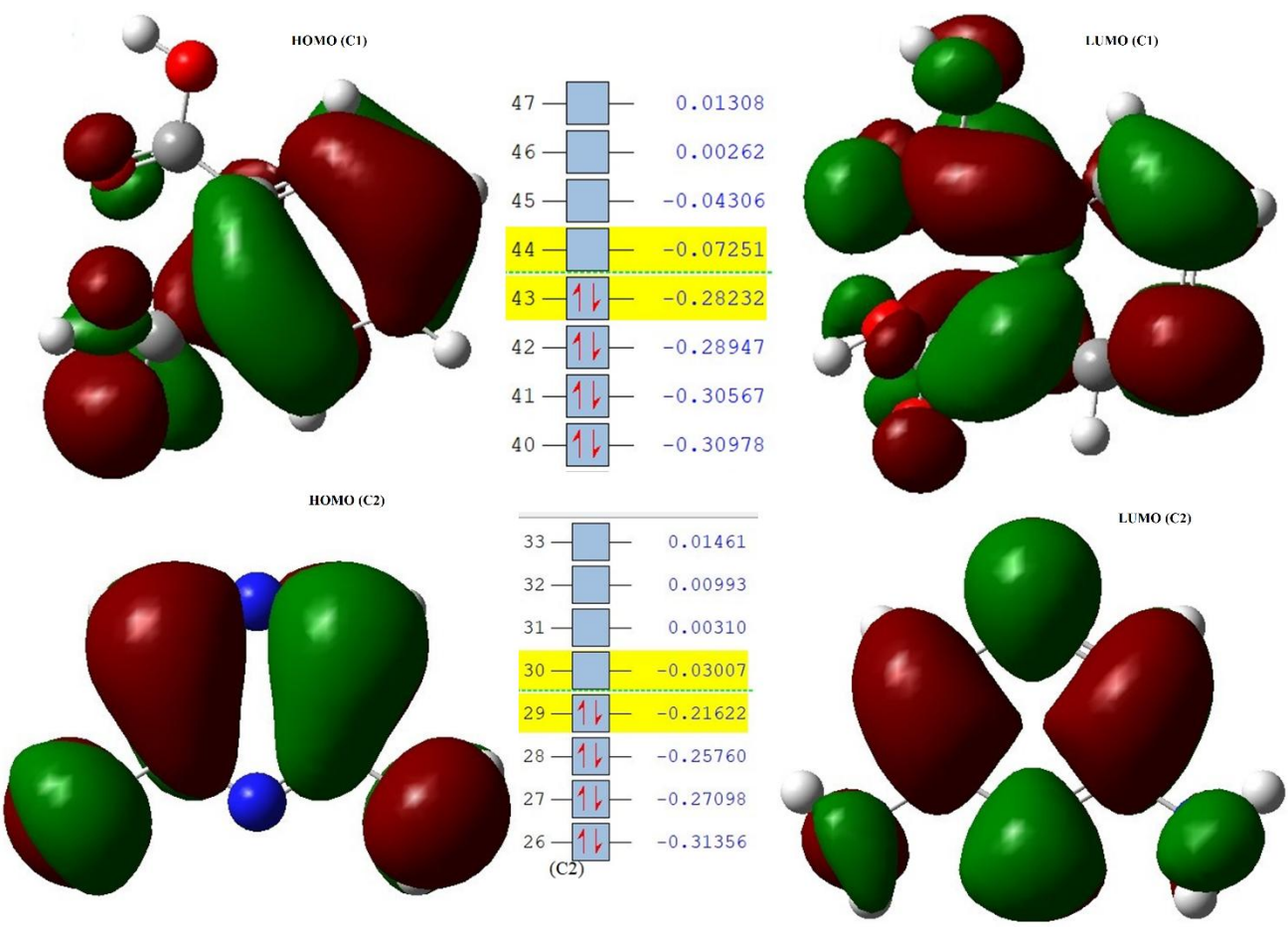

Fig. 2. The highest occupied molecular orbital (HOMO) and lowest unoccupied molecular orbital (LUMO) distributions of **C1** and **C2**. **C1** exhibited HOMO and LUMO energies of −0.28232 and −0.07251 eV, respectively, with an energy gap (ΔE) of 0.20981 eV. **C2** showed HOMO and LUMO energies of −0.21622 and −0.03007 eV, respectively, with a smaller energy gap of 0.18615 eV**.**

Table 4. GC–MS analysis of ethanolic and methanolic extracts of *F. arabica*.

S. No.	Solvent	Compounds	Retention time	Percentages (%)
1.	Ethanol	Formic acid	36.4	90.76
		Methyl diselenide	1.54	4.65
		Carbamicacid, n-(*N* cyanomethylpropanamide -2 y	3.87	0.49
		Pterin-6-carboxylic acid	4.36	0.63
		Nordiazepam	4.71	0.40
		methyl (Z)-octadec-9-enoate	5.11	1.98
		Di-n-octyl phthalate	6.8	1.09
2.	Methanol	2,2-dichloroacetamide	1.33	1.47
		Propanamide	1.36	19.9
		6-fluoro-2-[4-[(E)-2-phenylethenyl] phenyl]quinoline-4-carbox	3.72	27.99
		Acetic acid, hydrazine	4.68	3.35
		pyrazine-2, 6-diamine	5.08	1.38
		Phthalic acid, di(hept-3-yl) ester	6.9	5.48

Two compounds, C1 (Phthalic acid, di(hept-3-yl) ester) and C2 (pyrazine-2,6-diamine), were selected for further analysis, including quantum chemical and MD simulations to assess their suitability for druggable compounds based on their physicochemical and other medicinal properties.

Quantum chemical analysis of C1 and C2: The most important variables in quantum chemical research are the energies of the HOMO (π donor) and LUMO (π acceptor). These molecular orbitals are identified as frontier molecular orbitals (FMOs).

FMO analysis was executed to evaluate the chemical reactivity and electronic properties of C1 and C2 (Fig. 2). The HOMO and LUMO energy levels indicate distinct electronic characteristics for the two compounds. For **C1**, the HOMO and LUMO energies were −0.28232 and −0.07251 eV, respectively, and a HOMO–LUMO energy gap (ΔE) of 0.20981 eV. C2 revealed a HOMO energy of −0.21622 eV and a LUMO energy of −0.03007 eV, corresponding to a smaller energy gap of 0.18615 eV. The approximately 0.024 eV reduction in the HOMO–LUMO gap for C2 suggests a higher electronic polarizability and greater chemical reactivity compared with C1.

MEP analysis: The molecular electrostatic potential (MEP) is an important quantum-mechanical property intrinsically related to the electron density distribution. It provides a thorough insight into electrophilic and nucleophilic reactive centers and reveals inter- and intramolecular interaction mechanisms. Positive electrostatic potential regions appear from the nuclear attraction forces applied on hypothetical test protons. On the contrary, negative electrostatic potential areas are due to the cumulative attraction of electron density. It is usually denoted in red on the electrostatic potential maps. For C1, the electrostatic potential ranged from -5.268×10^{-2} to $+5.268\times10^{-2}$ a.u., with a total electrostatic range of 0.010536 a.u. Correspondingly, for C2, the electrostatic potential diverged from -6.668×10^{-2} to$+6.668\times10^{-2}$ a.u., with a total electrostatic range of 0.13336 a.u. The chromatic scale shows quantitative data of electron distribution, with red regions revealing electron-rich areas for nucleophilic attack, yellow showing moderately electron-dense regions, green indicating neutral areas and balanced charge distribution, and blue areas being electron-deficient as electrophilic interactions (Fig. 3). This order of electrostatic potential is red < yellow < green < blue, with declining electron density.

MEP surfaces show the potential electrophilic and nucleophilic sites of C1 and C2 (Fig. 3). The MEP of C1 ranged from approximately -6.67×10^{-2} to $+6.67\times10^{-2}$ a.u., whereas C2 exhibited -5.27×10^{-2} to $+5.27\times10^{-2}$ a.u., indicating a more uniform surface charge distribution. In C1, the negative electrostatic potential (red regions) is localized around the oxygen. The positive potential (blue regions) is distributed around the hydrogen atoms, showing favorable sites for hydrogen bonding. In C2, the negative electrostatic potential is present around the nitrogen atoms, and the positive potential is located near the amino hydrogen atoms. The oxygen-containing functional groups in C1 and the nitrogen in C2 constituted the reactive regions.

Table 5. Binding affinity(kcal/mol) of the selected ligands to the target protein.

S. No	Compound ID	Name	Binding affinity
1	C1	Phthalic acid	-- 5.16
2	C2	Pyrazine- 2,6 --diamine	-- 4.27

Molecular docking: The molecular docking binding affinity scores of the two selected compounds, C1 and C2, against the target protein are listed in Table 5. The two compounds exhibited favourable binding affinities, with docking scores of −5.16 kcal/mol and −4.27 kcal/mol, respectively. The binding affinity of phthalic acid was approximately 0.89 kcal/mol lower (more favorable) than that of pyrazine-2,6-diamine.

MD simulation: The structural stabilities of the apo protein and C1- and C2-bound complexes were evaluated using the root mean square deviation (RMSD) over a 100 ns MD simulation (Fig. 4). The apo protein reached equilibrium within the first 10–15 ns, followed by a relatively stable trajectory with a backbone RMSD between 3.2 and 4.2 Å, averaging 3.7 Å. A transient RMSD of nearly 4.7 Å was observed at approximately 30 ns.

For the C1–protein complex, the protein backbone RMSD gradually increased during the first 40–50 ns before stabilizing between 3.8 Å and 4.4 Å. The maximum RMSD was observed at 4.6 Å, with moderate conformations. The ligand RMSD was found between 2.5 and 4.0 Å, which may reveal conformational adjustments in the binding pocket.

The C2–protein complex exhibited equilibrium between 15–20 ns, with the protein RMSD of 3.5–4.3 Å for the whole simulation. The RMSD of C2 was consistently lower, between 2.3 and 3.2 Å, when compared with C1. The lower ligand RMSD shows that C2 demonstrated favorable binding in the pocket during the simulation.

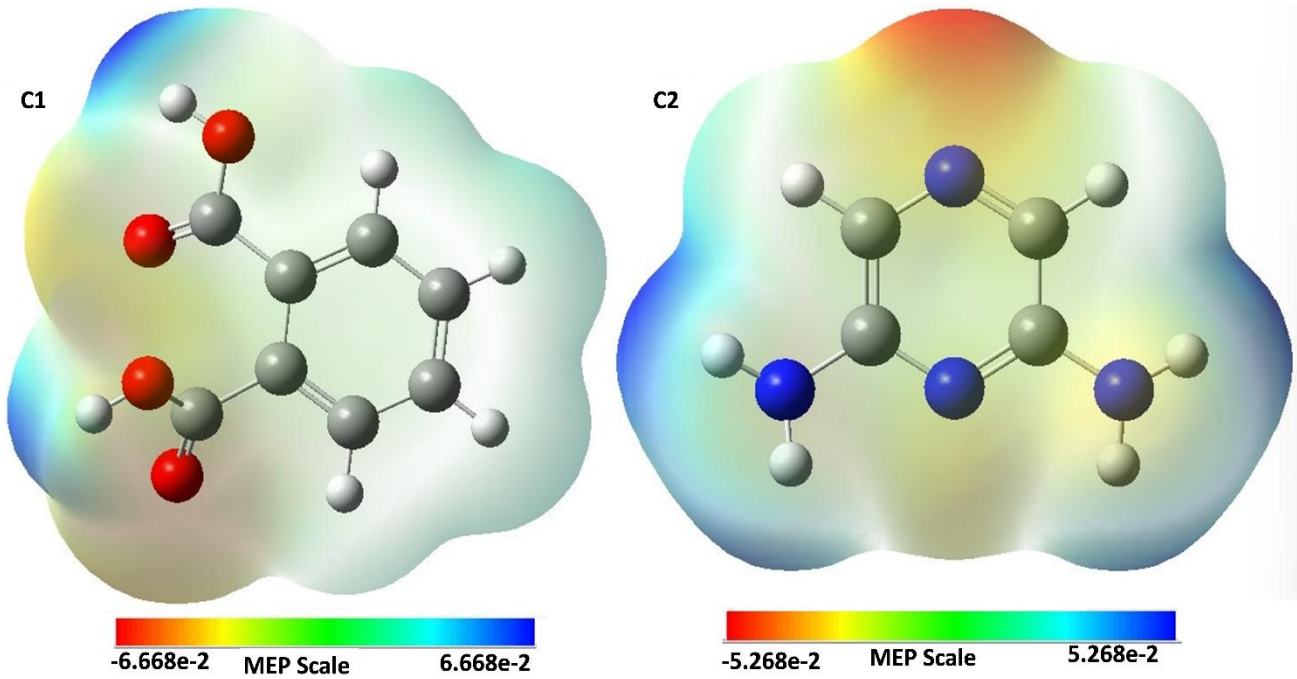

Fig. 3. MEP surfaces of C1 and C2. Red: electron-rich, blue: electron-deficient, and green/yellow: intermediate electrostatic potential.

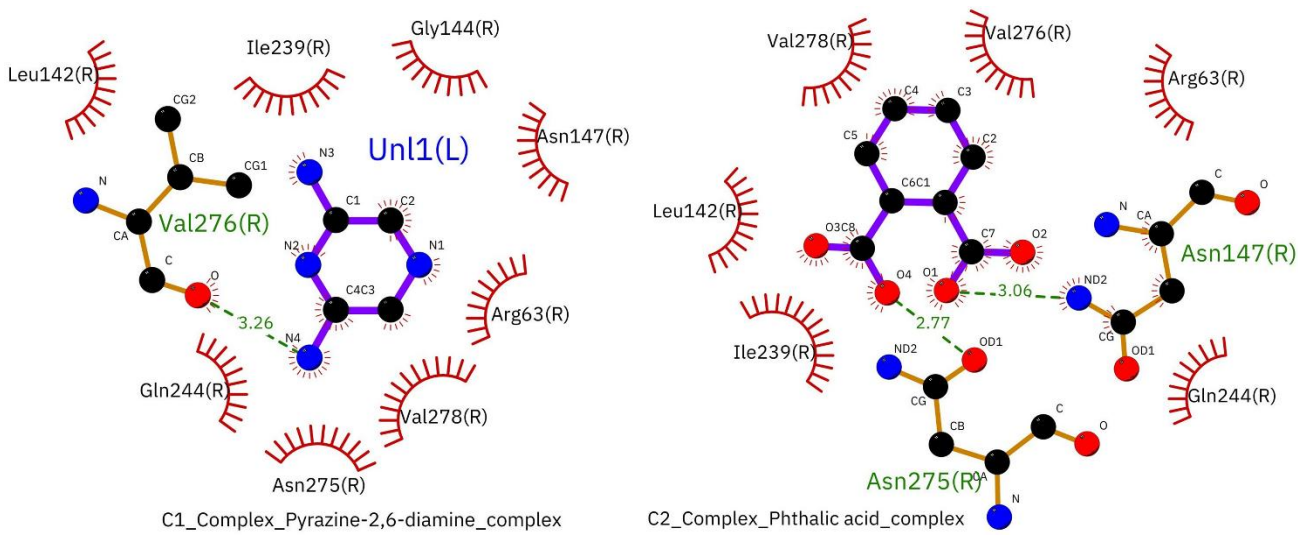

Fig. 6. Two-dimensional interaction diagrams of C1 (phthalic acid) and C2 (Pyrazine-2,6-diamine) bound within the active site. The green dashed lines indicate hydrogen bonds, and the red semicircular arcs represent hydrophobic interactions.

The residue-level flexibility and fluctuation of the apo protein and C1, C2-bound complexes were evaluated using root mean square fluctuation (RMSF) of the Cα atoms (See Fig. 5). The apo protein exhibited low RMSF (fluctuations) values predominantly from 1.0–2.0 Å. However, dominant fluctuations were observed in protein loop regions (residues 35-45, 85-120, and 125-135), with 5.0-7.4 Å RMSF values.

The binding of C1 may cause a rise in residue flexibility when compared to the apo protein. Most residues maintained RMSF values below 2.5 Å, while clear long peaks were observed near amino acid residues at 30–40, 90–100, 110–120, and 130–140, reaching a fluctuation to 9.0 Å. These increased flexibilities suggest that C1 may induce conformational changes in the flexible loop regions around the ligand-binding site and maintain the stability of the protein core.

The C2-bound complex exhibited less flexibility (fluctuations). The average RMSF was observed from 1.0 to 2.0 Å, with a few peaks around residues 35–40, 85–95, 110–120, and 130–140, reaching 8.0 Å. Compared with C1, several peaks were reduced, including in the central loop regions. The RMSF analysis demonstrated that C2 causes lower flexibility in the target protein than C1 with favourable binding stability in the pocket.

The protein–ligand interaction shows that C1 (Phthalic acid) and C2 (Pyrazine-2,6-diamine) occupied the same binding cavity and exhibited different interactions (Fig. 6). C1 established a single hydrogen bond with Val276 (Bond distance of 3.26 Å). The ligand was stabilized by different hydrophobic and van der Waals interactions with amino acids Leu142, Gly144, Ile239, Asn147, Arg63, Gln244, Asn275, and Val278 within the target binding pocket.

C2 exhibited a more complex interaction network with different amino acids of the target protein by forming two hydrogen bonds with Asn147 and Asn275 (bond distances: 2.77 Å and 3.06 Å, respectively). The ligand formed hydrophobic contact with Leu142, Ile239, Val276, Val278, Arg63, and Gly144, which may enhance its stability in the protein active site. These findings indicate that C2 exhibits better interaction patterns within the target protein active site.

Protein–ligand contact analysis was performed to evaluate residue-specific interactions (Fig. 7). For the C1 complex, the interactions were dominated by hydrogen bonds with Arg63, Gln244, Asn275, and Val276. Among these, Arg63 showed the highest interaction persistence (≈1.0), followed by Asn275 and Gln244. Moderate interactions were observed with Thr56 (≈0.53), Asn147 (≈0.58), and Gly144 (≈0.29). Gly54, Met55, Glu57, Asn58, Lys101, Leu142, Glu145, Gln148, Ile239, Phe277, and Val278 exhibited interaction fractions below 0.10.

Among the protein–ligand interactions, C2 showed a more diverse interaction network including hydrogen bonds. As shown in Fig. 7, Gln244 demonstrated the highest interaction pattern (≈0.99). Other interactions of C2 include Thr56 (≈0.95) and Met55 (≈0.74), Val276 and Asn275 showed intermediate interaction fractions (0.44 and 0.35, respectively). Other residues, including Asn57, Arg58, Lys99, Gly144, Ile239, and Val278, showed water-bridge interactions (0.15-0.30).

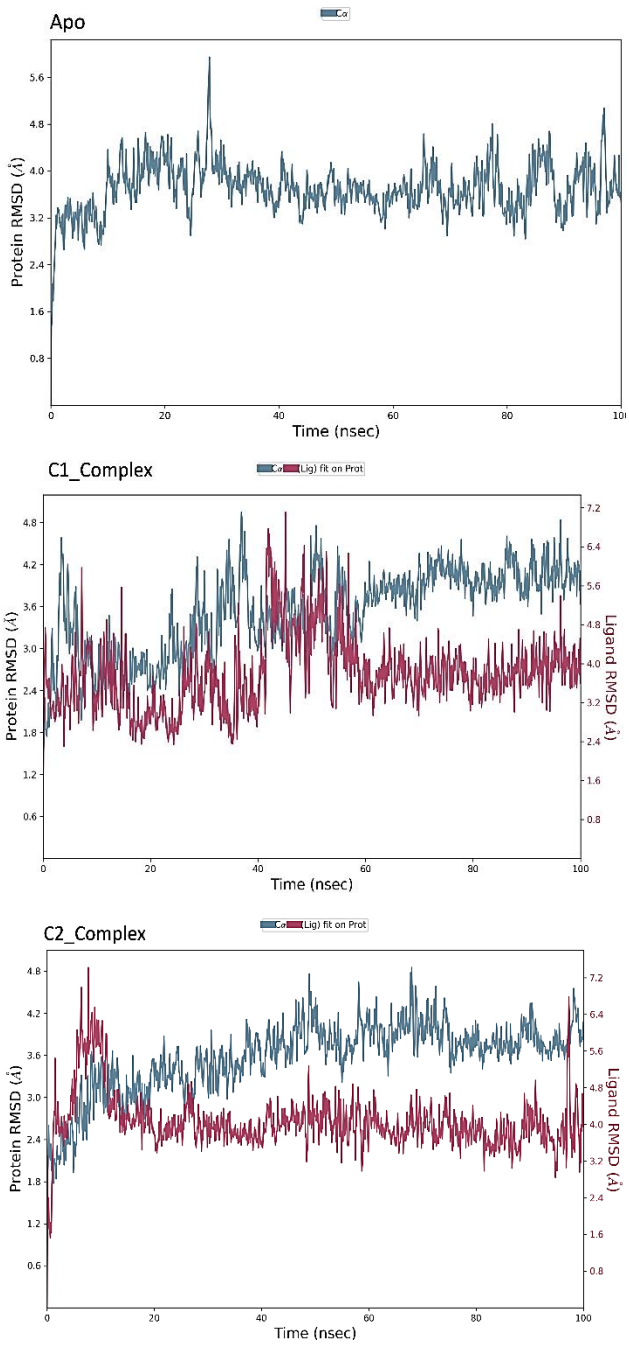

Fig. 4. Root mean square deviation of the apo protein and with C1- and C2 complexes. Left: Apo protein backbone RMSD. Right panels: Protein backbone RMSD (blue) and **C1** and **C2** complexes RMSD (red).

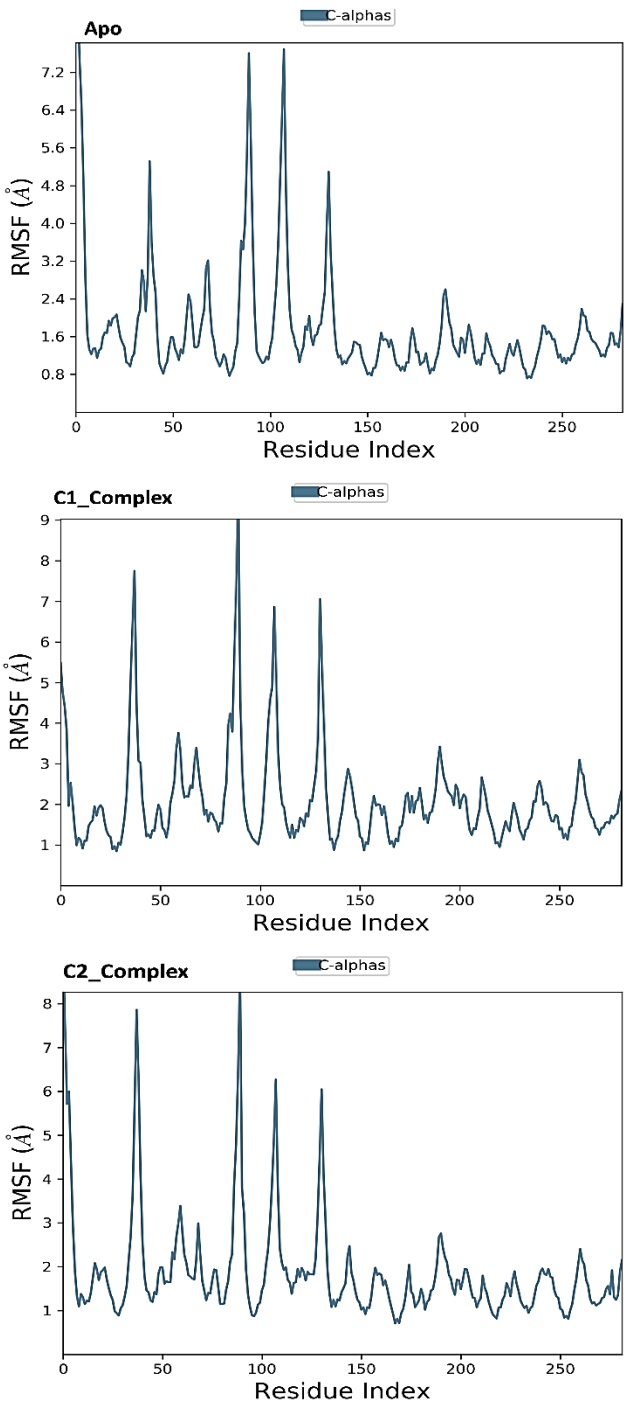

Fig. 5. Root mean square fluctuation of Cα of apo and ligand-bound C1 and C2 complexes.

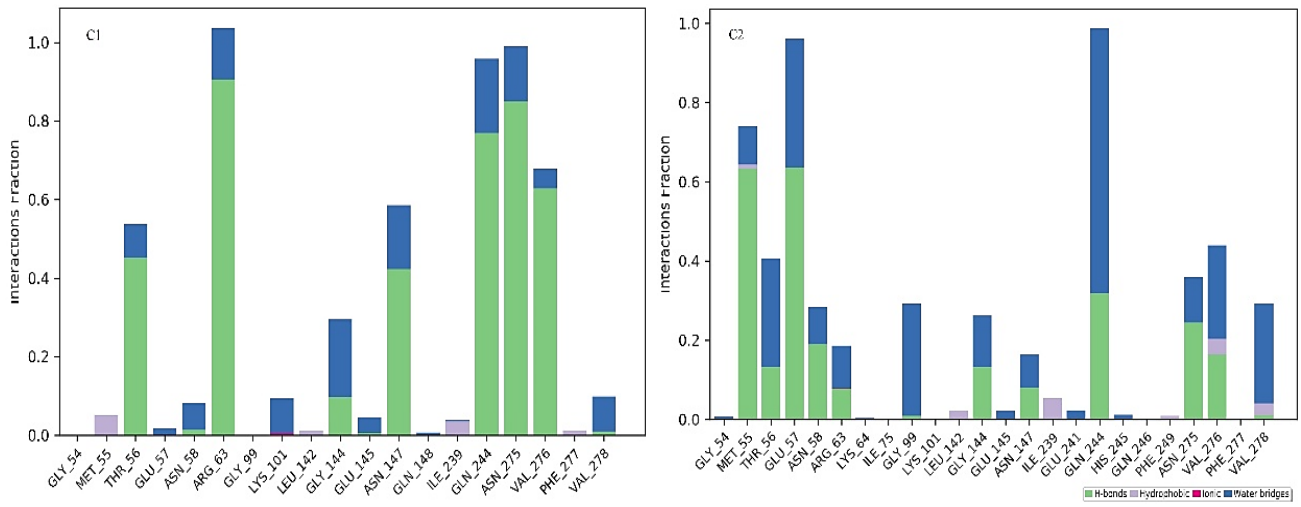

Fig. 7. Protein–ligand interaction fraction during the 100 ns molecular dynamics simulation. Blue: Hydrogen Bonds. Green (Light Green): π–π stacking interactions. Pink/Purple: Metal Complexes or Salt Bridges (ionic interactions).

The principal component analysis (PCA) and the dynamic cross-correlation matrix (DCCM) of the apo protein and C1-bound complex are shown in Fig. 8. PCA revealed differences in the motions between the two systems. For the apo protein, the first principal component (PC1) accounted for 20.85% of the total variance, while PC2 and PC3 contributed 15.42% and 10.06%, respectively. The C1-bound complex exhibited more dynamic from PC1 (44.08%), followed by PC2 (11.05%) and PC3 (7.75%), respectively.

The DCCM results of apo, C1- and C2-bound complexes demonstrated positive correlations along the diagonal (correlation coefficient ≈ +1.0). The off-diagonal areas exhibited varying degrees of correlated (0.3-0.8) motions. The C1 complex showed more positive correlations and a reduction in long-range anticorrelated motions.

The PCA and DCCM of the C2-bound complex are illustrated in Fig. 9. PCA showed that ligand binding significantly altered the collective motion of the protein. The C2-bound complex showed a greater contribution from PC1 (36.9%), while PC2 and PC3 contributed 11.62% and 11.20%, respectively, with a collective variance of 59.7% for the first three primary components.

The DCCM analysis revealed substantial differences in the residue–residue dynamic correlations between the apo and ligand-bound systems. Compared with the apo protein, the C2 complex exhibited a more positive correlation in long-range anticorrelated motions, mostly at residues surrounding the ligand-binding region.

Discussion

Persistent endodontic infections are a leading cause of root canal treatment failure. *E. faecalis* is one of the most frequently implicated microorganisms because of its ability to survive adverse intracanal conditions (Spíndola *et al.,* 2023). In the present study, *E. faecalis* was isolated and molecularly confirmed in 10/20 (50%) patients with endodontic treatment failure. This prevalence ratio falls within the 24% to 77% range as shown in previous studies (Khalifa *et al.,* 2016; Tong *et al.,* 2013). These differences are probably because of differences in topographical locations, prior antimicrobial exposure, and microbial detection techniques (Hoque *et al.,* 2023; Sharma *et al.,* 2025). These findings are consistent with those of another study reported in literature. They found that *E. faecalis* was present in 11 (45.8%) of 24 root canals (Pinheiro *et al.,* 2003).

The persistence of *E. faecalis* in root canal systems is mostly attributed to its ability to penetrate dentinal tubules, tolerate nutrient deprivation and alkaline environments, and form resilient biofilms. These characteristics enable microorganisms to resist conventional disinfection procedures and contribute to treatment failure (Ahmad *et al.,* 2024; Parga *et al.,* 2025). Therefore, there is increasing interest in identifying alternative antimicrobial agents that can overcome the limitations of existing endodontic disinfectants.

Antibiotic resistance is a serious issue in endodontics because it limits the choice of antibiotics used to treat infections. The results of the present study complete the antibiotic susceptibility of isolates against ampicillin and amoxicillin-clavulanate. A study in literature reported the susceptibility of amoxicillin-clavulanate as 100% while ampicillin was 50% among *E. faecalis* isolates from endodontic failure cases. (Sharma *et al.,* 2025) All isolates were resistant to tetracycline and vancomycin, whereas 80% to erythromycin. In accordance with our study, antibiotic resistance against tetracycline and erythromycin in *E. faecalis* has been observed (Kumar *et al.,* 2013). In contrast to our study, the literature has reported the sensitivity of all *E. faecalis* isolates to vancomycin (Endo *et al.,* 2014).

The inadequate antimicrobial activity of sodium hypochlorite and multidrug-resistant antibiotics against *E. faecalis* observed in the current study highlights the need for alternative antimicrobial approaches in endodontic treatment. The persistence of this pathogen, despite conventional treatment, has led to increased interest in phytochemical-based agents with enhanced antibiofilm properties (Alghamdi & Shakir, 2020).

The present study investigated the antimicrobial efficacy of *F. arabica* against *E. faecalis* isolated from failed endodontic cases. To the best of our knowledge, there is limited evidence regarding the activity of *F. arabica* against *E. faecalis* associated with endodontic infections. However, its antimicrobial effects against other bacterial species have previously been reported (Iftikhar *et al.,* 2022). Abobaker (2015) determined the antimicrobial activity of *F. arabica* methanol and distilled water extracts against Gram-positive and Gram-negative bacteria. The *Staphylococcus aureus* and *Staphylococcus dermis* were ineffective in distilled water; however, methanolic extracts showed 12 mm and 10 mm, respectively (Abobaker, 2015). The favorable efficacy of the ethanolic extract may be due to the efficiency of ethanol for moderately polar phytochemicals, including flavonoids, phenolic compounds, alkaloids, and tannins. The enhanced antimicrobial activity observed in the ethanolic extract is therefore likely due to the synergistic action of multiple bioactive constituents (Ali & Neelakantan, 2022; Iftikhar *et al.,* 2022).

The comparatively low antimicrobial activity of methanol may be due to differences in solvent polarity, which affect phytochemical extraction. The distilled water extract showed antibacterial effect because hydrophobic phytochemicals could limit solubility in water (Arya *et al.,* 2025). These differences may be attributed to variations in concentration, exposure time, inoculum density, and experimental conditions. Therefore, the results suggest that *F. arabica* may have favorable antimicrobial properties.

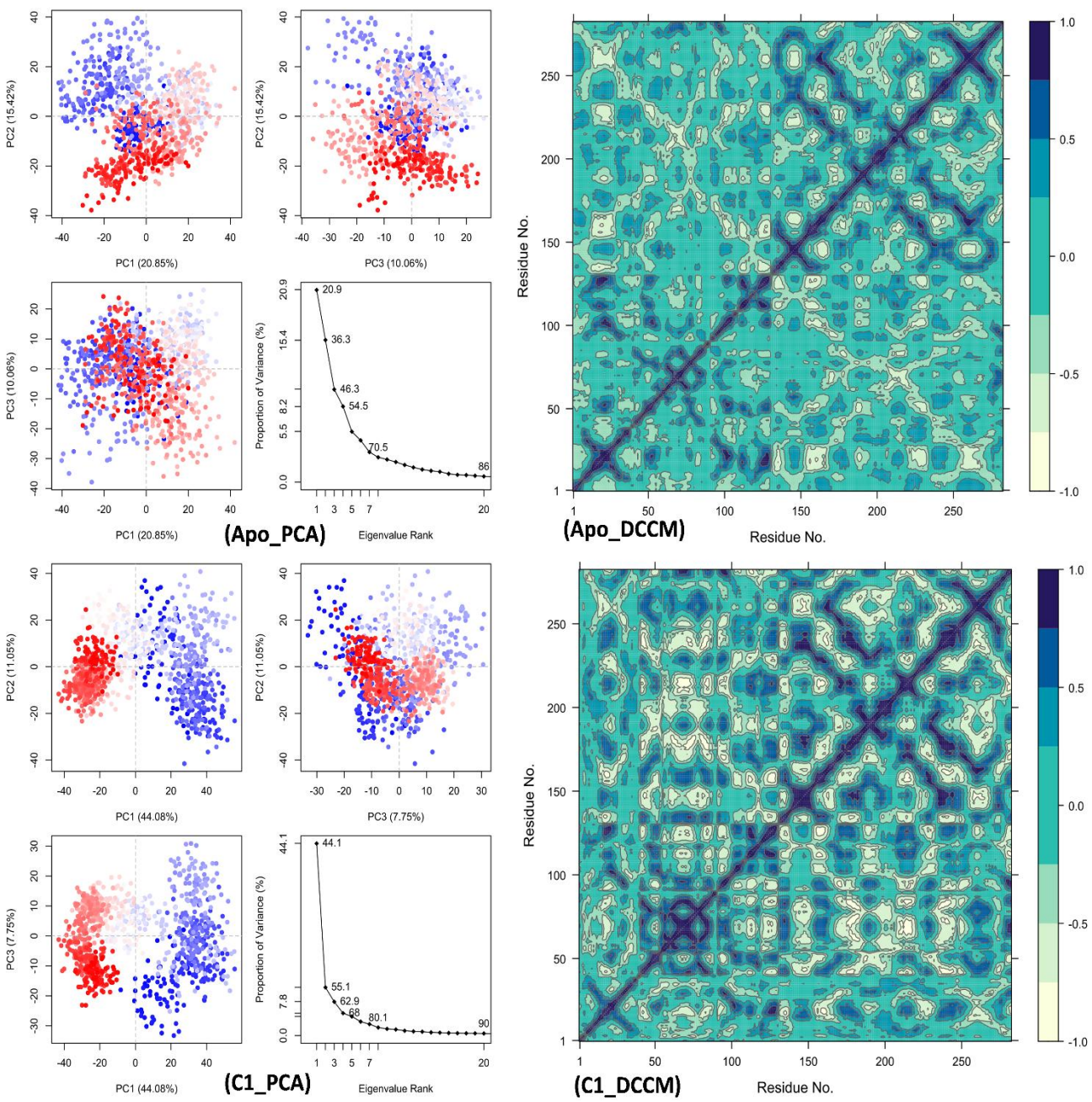

Fig. 8. Principal component analysis (PCA) and dynamic cross-correlation matrix (DCCM) of the apo protein and the C1-bound complex. The PCA score plots (PC1 vs. PC2) depict the conformational space sampled by the apo protein and C1 complex. In contrast, the scree plots illustrate the percentage variance explained by each PC and the cumulative variance.

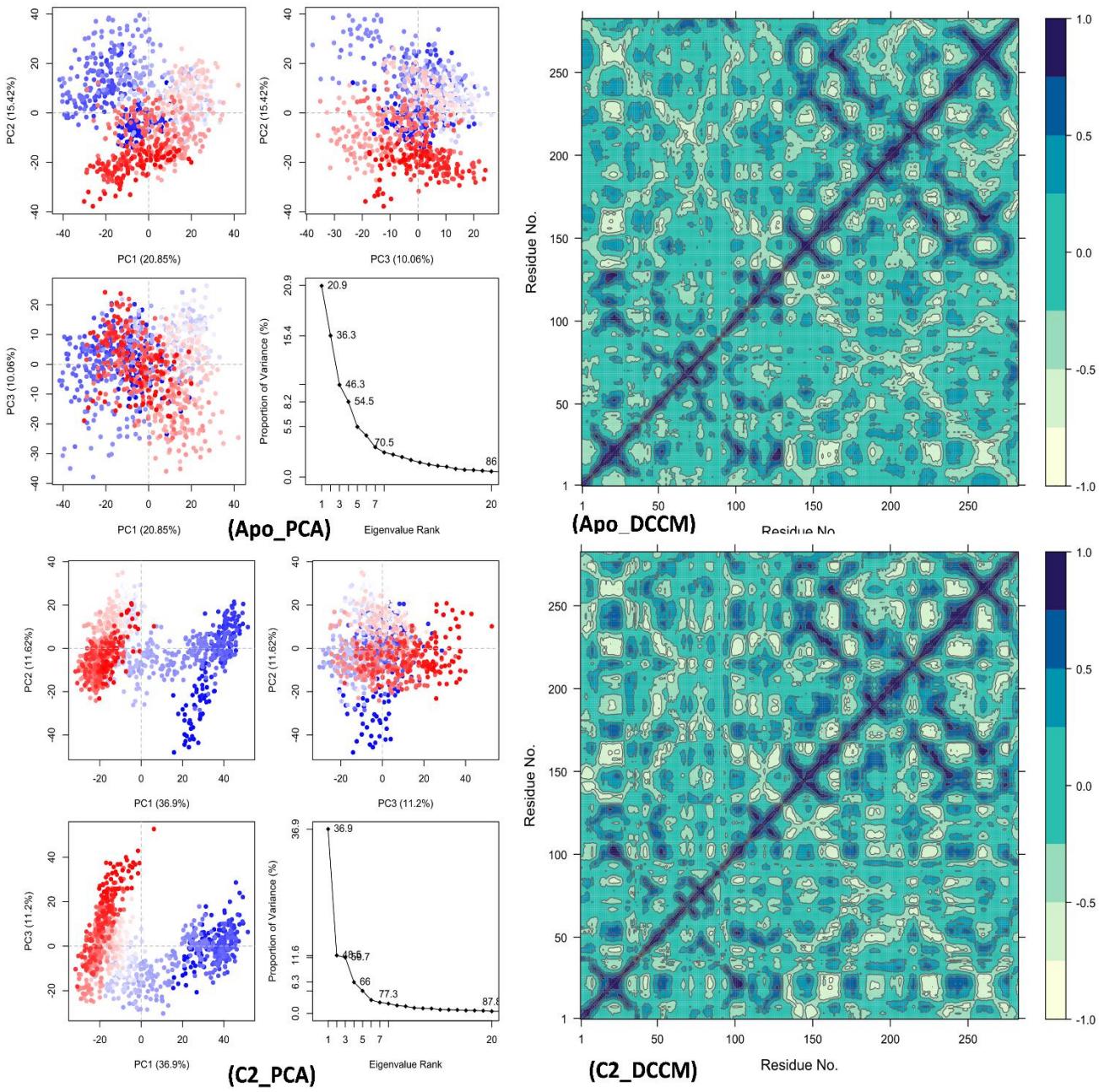

Fig. 9. Principal component analysis (PCA) and dynamic cross-correlation matrix (DCCM) of the apo protein and C2-bound complex. The PCA score plots (PC1 vs. PC2) illustrate the conformational space of the apo protein and C2 complex and show the percentage variance explained by each principal component and the corresponding cumulative variance.

Ace protein affects the persistent colonization and biofilm formation within the root canals (Tong *et al.,* 2013). The biological activity of medicinal plants is often attributed to synergistic interactions among multiple compounds. Therefore, the identified phytochemicals may collectively contribute to the observed antibacterial effect (Vaou *et al.,* 2022). To further explore the possible mechanism of action, molecular dynamics simulations were performed using the collagen adhesin Ace protein of *E. faecalis*.

The HOMO of C1 is distributed over the oxygen-containing functional groups, indicating that these regions are likely to participate in electron donation during intermolecular interactions. The LUMO is similarly localized, suggesting a favorable electron-accepting capability within the same molecular region. In C2, the HOMO was predominantly localized, indicating efficient intramolecular charge transfer. The smaller HOMO–LUMO gap of C2 implies a lower excitation energy and interactions with the target protein. These findings suggest that C2 possesses higher flexibility and reactivity than C1, which may contribute to its favourable biological activity.

The MEP analysis revealed charge distributions that influence the binding behaviors of C1 and C2. The comparatively narrower electrostatic potential of C2 suggests a more balanced charge distribution, which may facilitate stronger electrostatic complementarity with the receptor. MEP mapping has been widely used to identify reactive molecular regions and predict non-covalent interactions and binding affinity (Hasan *et al.,* 2025).

The consistently lower ligand RMSD of the C2 complex suggests reduced localized displacement within the binding pocket, whereas RMSF analysis showed that ligand

binding did not induce substantial fluctuations in the protein backbone, except for a few flexible loop regions. Furthermore, the protein–ligand contact fraction analysis identified persistent interactions with Arg63, Gln244, Asn275, and Val276 in the C1 complex, whereas Gln244, Thr56, Met55, Asn275, and Val276 remained highly occupied in the C2 complex throughout the simulation. These long-lived hydrogen bonds, hydrophobic contacts, and water-mediated interactions indicate stable ligand accommodation within the binding cavity and are important determinants of binding affinity and complex stability.

These PCA and DCCM results indicate that ligand binding promotes coordinated residue movement and strengthens the internal dynamic communication network of the protein. Collectively, PCA and DCCM analyses demonstrated that C1 induced a more compact conformational landscape and a more coherent correlation network, consistent with the enhanced structural stability observed from RMSD and RMSF analyses. Compared with the apo protein, the PCA score plots of the C2 complex exhibited more compact conformational clustering along PC1, suggesting that ligand binding effectively constrained the dominant collective motions and promoted a more stable conformational landscape (Xiong *et al.*, 2025).

The redistribution of correlated motions (Figures 8 and 9) indicates enhanced dynamic communication following ligand binding. Collectively, PCA and DCCM analyses demonstrated that C2 stabilizes the protein by reducing large-scale conformational fluctuations and strengthening coordinated residue motions, which is consistent with the RMSD, RMSF, and protein–ligand interaction analyses, which showed sustained binding stability throughout the molecular dynamics simulation.

The findings of the present study should be interpreted considering its limitations. First, only ten molecularly confirmed *E. faecalis* isolates were included in the downstream analyses, which may limit the generalizability of our results. Second, the antimicrobial assays were conducted *In vitro*, which does not fully replicate the complex root canal environment. Third, cytotoxicity, dentin penetration, biofilm disruption, and biocompatibility assessments were not performed in this study. Finally, molecular docking is a predictive computational approach that should be validated through molecular dynamics simulations and *In vivo* studies. are recommended.

Conclusion

This study demonstrated that *F. arabica* ethanolic and methanolic extracts possess favorable antibacterial activity against *E. faecalis* from endodontic failure cases. The ethanolic extract exhibited the most favorable antimicrobial efficacy as compared to 2.5% sodium hypochlorite and aqueous extracts. GC–MS analysis identified potentially active compounds. The molecular dynamics simulations provided mechanistic insights showing favorable interactions between selected phytochemicals and the Ace collagen-binding protein. These findings indicate that *F. arabica* could be a potential source of novel phytotherapeutic agents for endodontic applications. Further investigations involving larger sample sizes, biofilm disruption assays, cytotoxicity assessments, and *In vivo* or clinical evaluations are required before *F. arabica* can be considered for routine use in endodontic disinfection.

Acknowledgement

The authors thank and acknowledge all patients who participated in the study. We are thankful to the late Professor Aftab Ahmad and Miss Ayesha Saeed for providing technical support for the experiments.

Author's Contributions: Aneela Ejaz: Data acquisition, collection, and initial draft writing; Dr. Huma Sattar: Reviewing and editing; Dr. Muhammad Tahir Khan: Study design, writing the original draft, reviewing and editing; Dr Muhammad Hassan: Data analysis and interpretation and review of the draft.

Funding Statement: No funding was received from any agency, organization, or institution for this study; it was fully self-supported by the authors.

Data availability statement: The datasets generated during and/or analysed during the current study are available from the corresponding author on reasonable request.

Ethical approval: Ethical approval was obtained from the Institutional Review Board of the University of Lahore (IMBB/BBBC/23/140). Informed consent was obtained from all patients.

Conflict of Interest Disclosure: The authors report no conflicts of interest in the conduct or publication of this study.

References

Abobaker, D.M. 2015. Preliminary phytochemical analysis and antibacterial activity of the aqueous and ethanolic extracts of *Fagonia arabica* L., used as traditional medicinal plant in Libyan. *Int. J. Sci. Res.*, 6: 2319-7064.

Ahmad, M., S. Sohail, B. Khalid, U. Adeeb, M. Idrees and M. Memon. 2024. Evaluating the causes of root canal treatment failure in Southern Punjab, Pakistan. *Pak. Postgrad. Med. J.*, 35(3): 95.

Alghamdi, F. and M. Shakir. 2020. The influence of *Enterococcus faecalis* as a dental root canal pathogen on endodontic treatment: A systematic review. *Cureus*, 12(3): 1-10.

Ali, I.A.A. and P. Neelakantan. 2022. Antibiofilm activity of phytochemicals against *Enterococcus faecalis*: A literature review. *Phytother. Res.*, 36(7): 2824-2838.

Anonymous. 2024. Clinical and Laboratory Standards Institute (CLSI). Methods for dilution antimicrobial susceptibility tests for bacteria that grow aerobically (12th ed.). *CLSI Standard M07*, Clinical and Laboratory Standards Institute, Wayne, PA.

Arya, P., D. Vaidya, M. Kaushal, S. Devi, A. Gupta and S. Chand. 2025. Effects of different solvents on phytochemical constituents, in-vitro antimicrobial activity, and volatile components of *Boehmeria rugulosa* Wedd. wood extract. *Sci. Rep.*, 15(1): 29135.

Aydın, Z.U., D. Erdönmez and G. Akdemir Evrendilek. 2025. Can pulsed electric fields be an alternative for disinfection in endodontic treatment? *Appl. Sci.*, 15(20): 11133.

Azad, A., S. Rostamifar, F. Modaresi, A. Bazrafkan and Z. Rezaie. 2020. Assessment of the a0ntibacterial effects of bismuth nanoparticles against *Enterococcus faecalis*. *Biomed. Res. Int.*, 2020: 1-7.

Budala, D.G., M.A. Martu, G.A. Maftei, D.A. Diaconu-Popa, V. Danila and I. Luchian. 2023. The role of natural compounds in optimizing contemporary dental treatment—Current status and future trends. *J. Funct. Biomater*, 14(5): 273.

Butt, S., Y. Badshah, M. Shabbir and M. Rafiq. 2020. Molecular docking using Chimera and Autodock Vina software for non bioinformaticians. *JMIR Bioinform.*, 1(1): e14232.

Endo, M.S., F.G. Signoretti, V.S. Kitayama, A.C. Marinho, F.C. Martinho and B.P.F.A. Gomes. 2014. Culture and molecular detection of Enterococcus faecalis from patients with failure endodontic treatment and antimicrobial susceptibility of clinical isolates. *Braz Dent Sci*., 17(3): 83-91.

Francisco, P.A., P.I.D.G. Fagundes, J.C. Lemes-Junior, A.R. Lima, M.R.Z. Passini and B.P. Gomes. 2021. Pathogenic potential of *Enterococcus faecalis* strains isolated from root canals after unsuccessful endodontic treatment. *Clin. Oral Investig.*, 25(9): 5171-5179.

Ghosh, G., P. Panda, M. Rath, A. Pal, T. Sharma and D. Das. 2015. GC-MS analysis of bioactive compounds in the methanol extract of *Clerodendrum viscosum* leaves. *Pharmacog. Res.*, 7(1): 110-113.

Hasan, M., M.I. Hossain, N.H. Siddiquee, E. Ahmed, M.W.H. Talukder, M. Rahamatolla, T. Nahar, P.R. Paul, M.H. Suhag and M. Uzzaman. 2025. Computational design and cheminformatics profiling of omeprazole derivatives for enhanced proton pump inhibition of potassium-transporting ATPase alpha chain 1. *PLoS One*, 20(6): e0326655.

Hassoun, B.H. and G.J. Mohammed. 2022. Molecular genotyping of *Enterococcus faecalis* isolated from clinical sources by BOX-PCR and ERIC-PCR. *Int. J. Health Sci.*, 6(S1): 11664-11677.

Hoque, T., M. Hossain, S. Mahmud, A. Saleh and M.A.A. Moral. 2023. Rate of *Enterococcus faecalis* in saliva and failed root canal treated teeth—*In vivo* study. *Eur. J. Dent. OralHealth*, 4: 15-18.

Hubble, T.S., J.F. Hatton, S.R. Nallapareddy, B.E. Murray and M.J. Gillespie. 2003. Influence of *Enterococcus faecalis* proteases and the collagen-binding protein, Ace, on adhesion to dentin. *Oral Microbiol. Immunol.*, 18(2): 121-126.

Iftikhar, N., S.A.S. Chatha, T. Ahmad, Q. Ali, A.I. Hussain and H.A. Rathore. 2022. *Fagonia arabica* L.: A review of its phytochemistry, pharmacology and traditional uses. *Comb. Chem. High Throughput Screen*, 25: 1187-1199.

Iqbal, A. 2016. The factors responsible for endodontic treatment failure in the permanent dentitions of the patients reported to the college of dentistry, the University of Aljouf, kingdom of Saudi Arabia. *J. Clin. Diagn. Res.*, 5(10): 146-148.

Kalin, R., B. Karagülle, M.N. Açik, M. Karahan, Y. Öztürk and B. Çetinkaya. 2023. Investigation on antimicrobial resistance levels of *Escherichia coli* strains isolated from bovine fecal samples and comparison with guidelines of the Clinical Laboratory Standards Institute (CLSI) and European Committee on Antimicrobial Susceptibility Testing (EUCAST). *Kocatepe Vet. J.*, 16(3): 334-341.

Khalifa, L., M. Shlezinger, S. Beyth, Y. Houri-Haddad, S. Coppenhagen-Glazer, N. Beyth and R. Hazan. 2016. Phage therapy against *Enterococcus faecalis* in dental root canals. *J. Oral Microbiol.*, 8(1): 32157.

Kini, S., S.V. Shetty, K.H. Shetty, A. Kudva and P. Kumar. 2015. The efficiency of 2.5% sodium hypochlorite in preventing inoculation of periapical tissues with contaminated patency files: An *Ex vivo* evaluation. *J. Pharm. Bioallied Sci.*, 7(Suppl 2): S563-S566.

Kohli, M., S. Attavar, G. Mandavilli and N. Pallempati. 2026. Functional roles of virulence genes in adhesion, biofilm formation, and immune evasion of enterococcus faecalis. *Annals of Dental Specialty*, 14(2-2026): 60-67.

Kumar Patidar, R., M. Kumar Gupta and V. Singh. 2013. Phenotypic detection of virulence traits and antibiotic susceptibility of endodontic *Enterococcus faecalis* isolates. *Am. J. Microbiol. Res.*, 1(1): 4-9.

Li, S., D. Xiong, V.V. Klochkov, I.A. Khodov and X. He. 2025. Molecular dynamics reveals novel small-molecule inhibitors block PD-1/PD-L1 by promoting PD-L1 dimer stability. *Phys. Chem. Chem. Phys.*, 27(46): 24932-24947.

Mahmoud, N.N., A.E. Mekky, E. Mahmoud, M.M. El-Azab and M.I. Haggag. 2025. Insight into the biological activities of *Fagonia arabica* L. and its phytochemical constituents. *AMB Express*, 15: 114.

Mohsin, M.A., R.H. Jehad and M.W. Ameen. 2025. The antimicrobial characteristics of some natural remedies in root canal disinfection and artificial intelligence (AI): A review. *J. Port. Sci. Res.*, 8(4): 386-395.

Muhammad, Z., N.R. Hakila, A. Zulfiqar, Aymaska and K.A. Seemab. 2025. *In vitro* assessment of antibacterial, antioxidant, antifungal and anti-inflammatory activities of crude fruit extract of *Nigella sativa*: Research article. *Pak-Euro J. Med. Life Sci.*, 8(2): 453-462.

Nallamilli, L.S.R., K. Sirisha, H.P.K. Pilli, R.K. Konagala, Anwarullah and V. Chandolu. 2026. Antimicrobial efficacy of chitosan nanoparticles as intracanal medicament against *Enterococcus faecalis* and *Staphylococcus aureus*: An *In vitro* study. *J. Conserv. Dent. Endod.*, 29(4): 440-445.

Parga, A., J. Mattu, G.N. Belibasakis, K.A. Kline, J.G. Leprince and D. Manoil. 2025. A polymicrobial perspective into the ecological role of *Enterococcus faecalis* in dental root canal infections. *npj Biofilms Microbiomes*, 11(1): 83.

Pinheiro, E.T., B.P.F.A. Gomes, C.C.R. Ferraz, F.B. Teixeira, A.A. Zaia and F.J. Souza Filho. 2003. Evaluation of root canal microorganisms isolated from teeth with endodontic failure and their antimicrobial susceptibility. *Oral Microbiol. Immunol.*, 18(2): 100-103.

Sharma, J., S. Jhamb, M. Mehta, J. Bhushan, S.B. Bhardwaj and A. Kaur. 2025. Prevalence of *Enterococcus faecalis* in refractory endodontic infections: A microbiological study. *J. Conserv. Dent. Endod.*, 28(5): 462-467.

Skotniczny, M. and P. Satora. 2023. Molecular detection and identification of plant-associated *Lactiplantibacillus plantarum*. *Int. J. Mol. Sci.*, 24(5): 4853.

Spíndola, L.C.P., A.M. Oliveira, D. Masterson, L.C. Maia and R.M.D. Souto. 2023. Prevalence of *Enterococcus* species in adults with periodontal health or with periodontitis: a systematic review. *Braz. J. Oral Res.*, 37: e019.

Tong, Z., J. Ling, Z. Lin, X. Li and Y. Mu. 2013. The effect of MTADN on 10 *Enterococcus faecalis* isolates and biofilm: An *In vitro* study. *J. Endod.*, 39(5): 674-678.

Tsimidou, M.Z. 2023. On the importance of the starting material choice and analytical procedures adopted when developing a strategy for the nanoencapsulation of saffron (*Crocus sativus* L.) bioactive antioxidants. *Antioxidants*, 12(2): 496.

Vaou, N., E. Stavropoulou, C. Voidarou, Z. Tsakris, G. Rozos, C. Tsigalou and E. Bezirtzoglou. 2022. Interactions between medical plant-derived bioactive compounds: Focus on antimicrobial combination effects. *Antibiotics*, 11(8): 1014.

Wallace, A.C., R.A. Laskowski and J.M. Thornton. 1995. LIGPLOT: A program to generate schematic diagrams of protein–ligand interactions. *Protein Eng.*, 8(2): 127-134.

Zou, X., X. Zheng, Y. Liang, C. Zhang, B. Fan, J. Liang, J. Ling, Z. Bian, Q. Yu, B. Hou, Z. Chen, X. Wei, L. Qiu, W. Chen, W. He, X. Xu and L. Yue. 2024. Expert consensus on irrigation and intracanal medication in root canal therapy. *Int. J. Oral Sci.*, 16(1): 23.

Zubair, M., F.D.R.S. Shakila, Z. Aisha and A.S. Khan. 2025. *In vitro* assessment of antibacterial, antioxidant, antifungal and anti-inflammatory activities of crude fruit extract of *Nigella sativa*: Research article. *Pak.-Euro J. Med. Life Sci.*, 8(2): 453-462.